Bending and buckling of wet paper

Minhee Lee, Seungho Kim, Ho-Young Kim, and L. Mahadevan

Citation: Physics of Fluids **28**, 042101 (2016); doi: 10.1063/1.4944659
View online: http://dx.doi.org/10.1063/1.4944659
View Table of Contents: http://scitation.aip.org/content/aip/journal/pof2/28/4?ver=pdfcov
Published by the AIP Publishing

PHYSICS OF FLUIDS **28**, 042101 (2016)

Bending and buckling of wet paper

Minhee Lee,[1] Seungho Kim,[1] Ho-Young Kim,[1,a)] and L. Mahadevan[2,b)]
[1]*Department of Mechanical and Aerospace Engineering, Seoul National University, Seoul 08826, South Korea*
[2]*Department of Physics and School of Engineering and Applied Sciences, Harvard University, Cambridge, Massachusetts 02138, USA*

(Received 4 October 2015; accepted 20 January 2016; published online 1 April 2016)

Flat paper stained with water buckles and wrinkles as it swells and deforms out of the original plane. Here we quantify the geometry and mechanics of a strip of paper that swells when it imbibes water from a narrow capillary. Characterizing the hygroexpansive nature of paper shows that thickness-wise swelling is much faster than in-plane water imbibition, leading to a simple picture for the process by which the strip of paper bends out of the plane. We model the out-of-plane deformation using a quasi-static theory and show that our results are consistent with quantitative experiments. © *2016 AIP Publishing LLC.* [http://dx.doi.org/10.1063/1.4944659]

I. INTRODUCTION

Materials can deform due to various external stimuli—thin films wrinkle when heated[1] or bombarded by ions,[2] polymers deform when irradiated by UV[3] or when they imbibe solvents,[4,5] and natural cellulose sponges swell by water absorption.[6] At an everyday level, we are accustomed to seeing paper deform when wet—for example, it curls or wrinkles when left in an environment of varying humidity or when placed on a moist environment.[7–9] Paper is composed of a network of cellulose fibers which are infiltrated by water that fills the hydrophilic fiber walls and the space between microfibrils.[10] This leads to the expansion of the inter-fiber space, causing the swelling and the growth of the fiber[11] and a simultaneous decrease in the stiffness of the paper.[12]

For slender sheets, there are two imbibition time scales: one that characterizes the rate at which gradients in swelling across the sheet are set up and eventually relax and a second that characterizes the rate at which gradients in swelling are set up and relax along the sheet. For dense sheets with low permeability, the transverse gradients cause sheets to curl and behave like a bimetallic strip,[13] while for porous sheets like those in ordinary paper, water imbibition occurs fairly rapidly along the transverse direction and eventually leads to swelling mediated by a slowly spread wetting front along the plane of paper that changes its length and thus causes it to bend and buckle. In this paper, we focus on this latter phenomenon using a simple model system where a strip of filter paper is suspended between two clamped supports while water emanating from a narrow capillary spreads out from the center of the paper bridge. This is one of the simplest configurations where we can explore the time-dependent buckling of wet paper driven by progressive wetting, as shown in Fig. 1. This process occurs as a combination of length- and thickness-wise water impregnations, the consequent swelling and softening of paper, and global deflection of the strip. We use experiments to dissect these physical ingredients and then construct a theoretical model to predict the shape evolution of wet paper.

II. CHARACTERIZATION OF HYGROEXPANSIVE RESPONSES

We used a filter paper (Whatman Grade 1) with an average thickness of 180 μm thickness. Paper is anisotropic with two principal directions in its plane, the machine direction (MD) and the

a)Electronic address: hyk@snu.ac.kr
b)Electronic address: lm@seas.harvard.edu

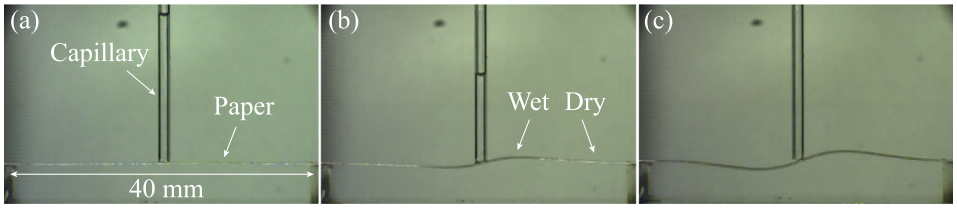

FIG. 1. Deflection of a suspended paper strip with capillary imbibition of water from a tube. (a) Initially dry paper at time $t = 0$. (b) Partially wet paper at $t = 8$ s. The wet region is darker than the dry one. (c) Fully wet paper at $t = 66$ s.

cross direction (CD).[14] The MD coincides with the direction of paper machine used in the sheet forming process and CD is perpendicular to it. In the thickness direction, several fiber layers are pressed during fabrication as shown in Fig. 2, the cause of the anisotropy. We placed a narrow paper strip, 5 mm in width, cut either in MD or CD on two supports as shown in Fig. 3(a) and supplied water from a tube gently touching the paper surface. Water infiltrates the paper due to capillary action until the paper is saturated and fully stretched. This allows us to measure the hygroexpansive strain of paper in various directions using images acquired by a CMOS camera (Photron SA1.1).

Figure 3(b) shows the temporal evolution of the strain in the CD for different lengths of the paper strips. Because it takes longer for water to reach the ends of longer strips, the time over which the hygroexpansive strain ϵ_c reaches its steady state value increases with the strip length. At saturation, ϵ_c is found to be $1.56 \times 10^{-2} \pm 0.15 \times 10^{-2}$. In contrast, the strain in MD $\epsilon_m = 0.32 \times 10^{-2} \pm 0.12 \times 10^{-2}$, which is less than ϵ_c, due to the anisotropy induced by stretching along the MD. We also measured the transient hygroexpansive strain in the thickness direction at different locations from the center of the tube, x, with the results shown in Fig. 3(c). At saturation, $\epsilon_t = 26.5 \times 10^{-2} \pm 2.2 \times 10^{-2}$. Plotting the time, t_s (in seconds), defined as the time taken for ϵ_t to reach 90% of its saturated value, versus x (in mm) as in Fig. 3(d), we find that

$$t_s \approx 3.56 \times 10^4 x^2. \tag{1}$$

In the absence of a theory for (1), we use it as an empirical relation together with the fact that thickness-wise swelling is faster than length-wise wicking to eventually derive the relation linking swelling to bending. In addition to the strains, we measured the weight ratio of water at saturation ϕ_s by supplying water from a capillary tube to a 1 cm-long paper strip, defined by $\phi_s = (m_s - m_d)/m_s = 0.63 \pm 0.005$, where m_d and m_s are the mass of the dry and the saturated paper, respectively. This allows us to relate Young's modulus, E, of the filter paper to its wetness by measuring the tensile stress and strain in CD using a tensile meter (Instron Model 5543). We first wetted the paper strip (10×30 mm^2 in area) at different locations with a pipette containing a pre-defined volume of water and waited for water to spread out evenly before measuring E at least 3 times for the same water weight ratio. Then the tensile test gives E as a function of ϕ as shown in Fig. 4; Young's modulus of the dry paper is $E_d \approx 828$ MPa, but it drops dramatically when even slightly wet, with $\phi = 0.1$, which is only 16% of ϕ_s, the saturated volume fraction of wet paper. We see that paper softens strongly with little absorption of water, but further wetting does not see a large change in E. For a fully wet paper, $E_s \approx 24$ MPa, which is 2.9% of that of a dry paper.

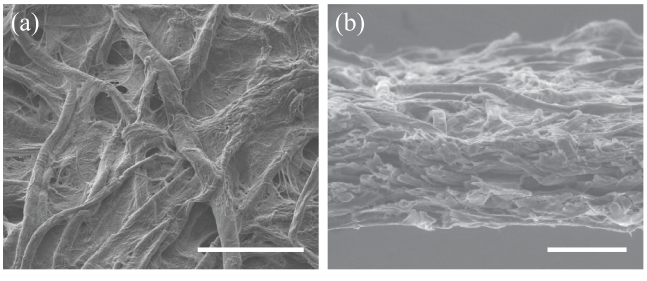

FIG. 2. Scanning electron microscopy images of a filter paper used in the experiments. (a) Top view. (b) Tilted view. Scale bars, 100 μm.

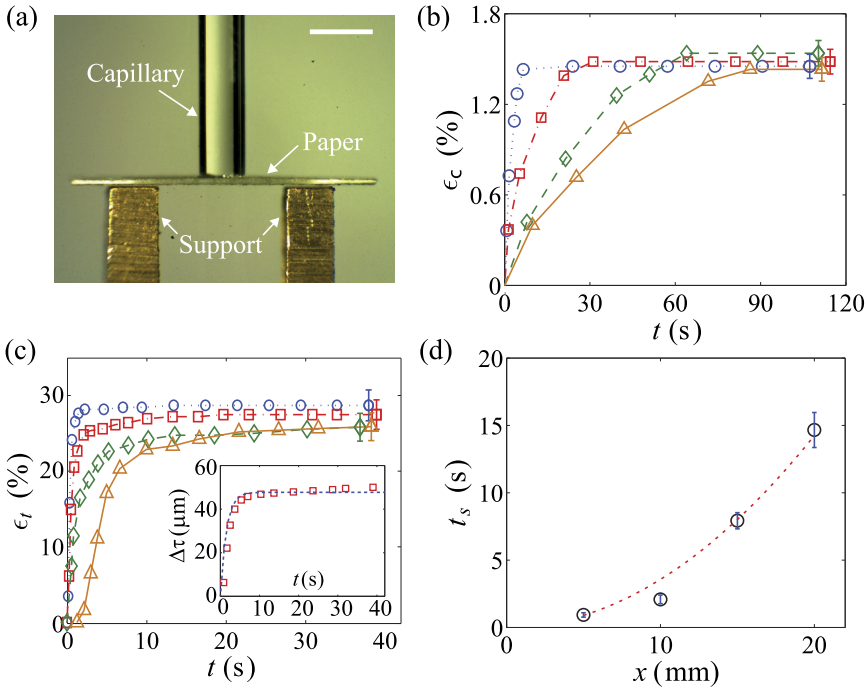

FIG. 3. Measurement of hygroexpansive strain by comparison of the dry and the wet paper. (a) Experimental setup to measure the strains. Scale bar, 2 mm. (b) The strain in CD, ϵ_c, of various lengths of the filter paper versus time. Circles, squares, diamonds, and triangles correspond to the strips 10, 20, 30 and 40 mm long, respectively. (c) The strain in thickness, ϵ_t, versus time measured with a paper strip of 40 mm in total length. The measurements were made at $x = 5$ mm (circles), 10 mm (squares), 15 mm (diamonds), and 20 mm (triangles). In the inset, we compare the measurement results for $x = 10$ mm with a curve corresponding to Eq. (2). (d) The settling time, t_s, of ϵ_t versus x.

To characterize the water imbibition dynamics, we measured the propagation of the water front as it emanates from the capillary once it gently touches the paper strip of width $b = 5$ mm. The water front reaches the paper sides and the opposite face at $t_1 = 190$ ms and $t_2 = 3$ ms, respectively. For $t \gg t_c = \max\{t_1, t_2\}$, the imbibition becomes virtually one-dimensional, as shown in Fig. 5(a). The one-dimensional propagation of the wetting front follows a Washburn-like behavior[15] in Fig. 5(b), with L_w the distance of the wetting front from the center of the tube given by $L_w = (D_w t)^{1/2}$, where $D_w = 7.8 \times 10^{-6}\ \mathrm{m}^2/\mathrm{s}$.

To evaluate the effect of thickness-wise swelling on length-wise imbibition, we model the thickness profile of a partially wet paper along the length using empirical relation (1). We first

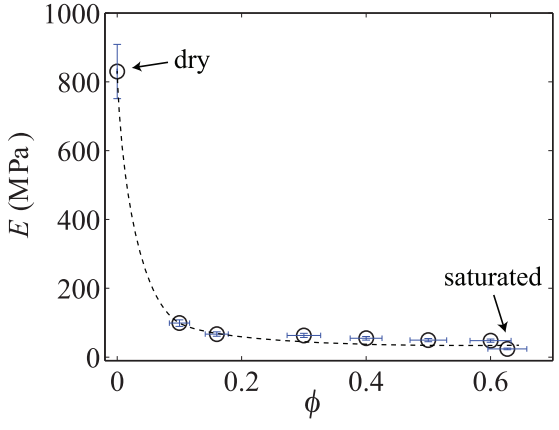

FIG. 4. Young's modulus of the filter paper in CD as a function of the water weight ratio, ϕ.

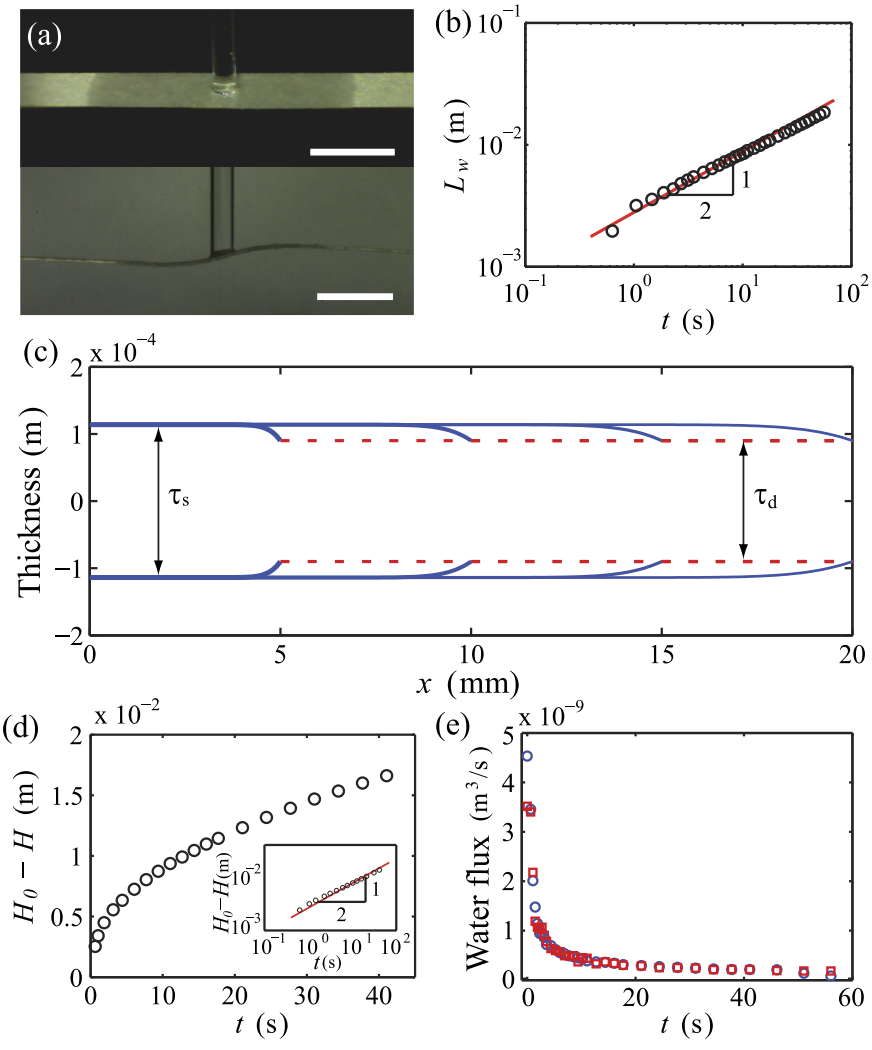

FIG. 5. Imbibition of water in paper. (a) The one-dimensional spreading of the water front. The upper and lower panels are tilted and side views at $t = 7.8$ s, respectively. Scale bars, 5 mm. (b) The distance of wet front from the tube center, L_w, that grows like $t^{1/2}$. (c) The calculated thickness profile of a partially wet paper for L_w= 5, 10, 15, and 20 mm. The blue solid line and red dashed line correspond to the wet and the dry region, respectively. (d) The change of height of the water column in the tube, plotted as $H_0 - H$ versus time. (e) Flow rates q_1 (blue circles) and q_2 (red squares) versus time.

assume that the thickness change, $\Delta\tau = \tau - \tau_d$, with τ the thickness of paper at x after time $\hat{t}$ has elapsed since the wetting front arrived and τ_d the thickness of the dry paper, can be described by $\Delta\tau/\Delta\tau_s = 1 - \exp(-k\hat{t})$, where $\Delta\tau_s = \tau_s - \tau_d$ with τ_s being the thickness of the saturated paper, as shown in Fig. 3(c). Then the thickness of paper at x is $\tau(x,t) = \tau_d + \Delta\tau(x,t)$. Since the paper at position x meets water at the time $T = x^2/D_w$, $\Delta\tau = 0$ for $t < T$ and

$$\frac{\Delta\tau(x,t)}{\Delta\tau_s} = 1 - \exp\left[-k\left(t - \frac{x^2}{D_w}\right)\right], \tag{2}$$

for $t > T$. In Fig. 5(c), we show the thickness profile for various L_w and find that the wet paper has a uniform thickness τ_s for most of the length, with a small transition zone that grows only weakly with L_w. Thus, we can approximate the flow as akin to capillary-driven imbibition through a porous medium with a constant cross-sectional area $b\tau_s$ with Washburn-like dynamics.

Indeed, in Fig. 5(d), when we plot the change of height of the water column in the tube, $H_0 - H$, where H_0 is the initial height of the water, with time, we see that it increases as $t^{1/2}$. Comparing the flow rate from the tube with an inner radius of $a = 0.57$ mm, $q_1 = -\pi a^2 \dot{H}$, and the

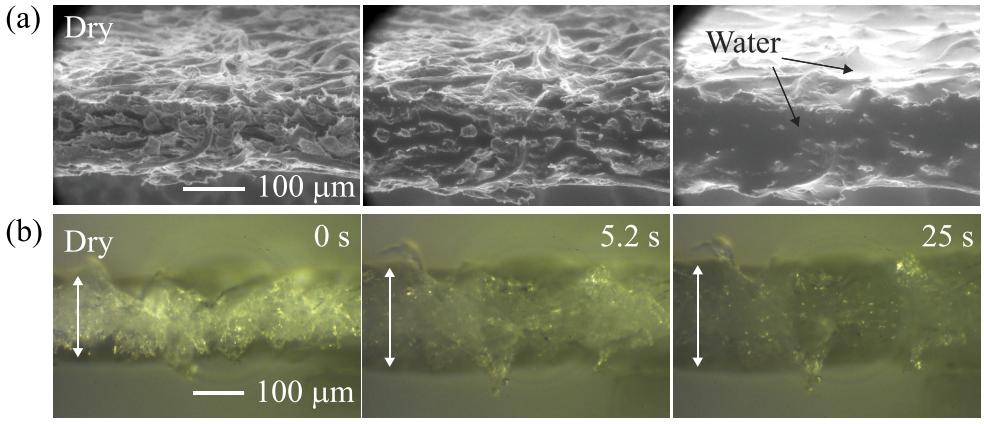

FIG. 6. Images of cross section of filter paper at different moisture contents. (a) ESEM (Environmental Scanning Electron Microscopy) images of paper being gradually wetted with increasing humidity. (b) Close-up images of paper strip in the experimental setup of Fig. 3(a) at 20 mm from the origin, where the capillary touches the paper strip at −51 s. The wet front is located just left to the image at time 0 s and progresses to the right with time. The white arrows indicate approximate thickness of the paper.

flux through the wet paper, $q_2 = 2nb\tau_s\dot{L}_w$, in Fig. 5(e), we find that $n = 0.49$, and $nb\tau_s$ corresponds to the effective cross-sectional area. It is useful to note that there is a difference between n, the ratio of water influx from the source to water flux through wet cross section, and $\hat{n}$, the porosity of saturated paper at steady state. The water weight ratio at saturation ϕ_s can be related to $\hat{n}$, the ratio of fluid volume to the total volume of the saturated porous paper, as

$$\phi_s = \frac{\hat{n}\rho_w}{\hat{n}\rho_w + (1-\hat{n})\rho_p}, \tag{3}$$

where ρ_w is the density of water, and ρ_p is an approximate density of dry fibers (1500 kg/m^3).[14] Substituting $\phi_s = 0.63$ as measured above gives $\hat{n} \approx 0.72$, which is greater than $n = 0.49$. We attribute this difference to the gradual relaxation of cellulose fiber structure with water absorption; although the thickness and Young's modulus of paper approach those for saturated paper shortly after being wet, paper is capable of absorbing more water over a relatively long period of time until saturation. In Fig. 6, we see that as the cross section of filter paper becomes gradually wet, both the environmental scanning electron microscopy (ESEM) (a) and the optical (b) images confirm that, while the second and third panels show insignificant difference in thickness, the surfaces are fully covered with water eventually. Thus, the existence of water at the surface plays an important role in making $\hat{n} > n$.

Our study of the hygroexpansive characteristics of paper shows that the swelling of paper and its consequent softening occur much faster than liquid imbibition except at the extremely early stages. Hence, during water impregnation, we can effectively assume that the wet portion instantaneously assumes the thickness τ_s and Young's modulus E_s. These findings allow us to decouple the deformation process from the hygroexpansive swelling dynamics, so that the elastic response of the paper strip caused by hygroexpansive swelling is limited by the slow capillary imbibition process which provides wetted length with a constant cross-sectional area at each instant.

III. POST-BUCKLING OF WET PAPER

To predict the temporal shape evolution of the paper strip using the rate of water imbibition, we now turn to a theoretical account of the process. Figure 7 shows the coordinate system to account for the observations in Fig. 1. We assume one-dimensional infiltration of water along the X-direction and use symmetry to consider the half-domain of length L from the pinned origin where the tube touches the paper to the clamped end. We note that the surface tension of the liquid holds the paper beam in contact with the capillary and prevents snapping from the nominally unstable second mode of buckling.[16]

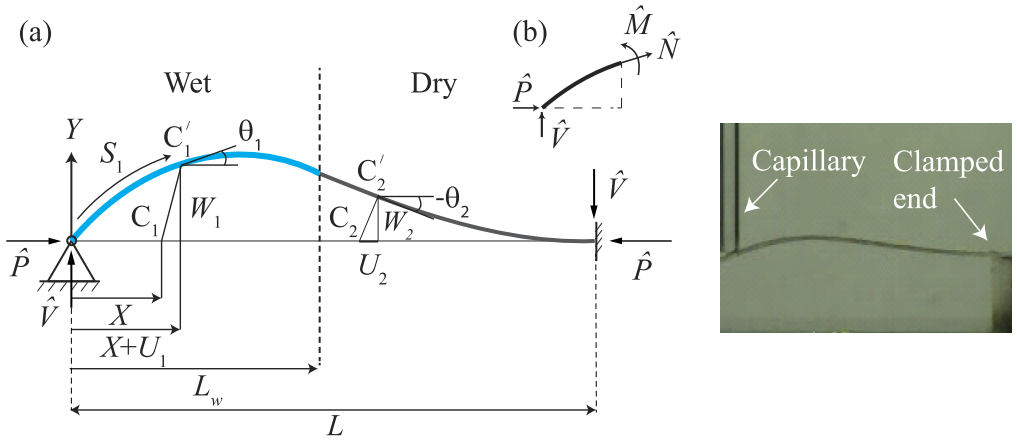

FIG. 7. (a) The coordinates system for a buckled paper strip consisting of wet and dry domains whose interface moves with time. The points C_1 and C_2 move to C_1' and C_2', respectively, by deformation. The experimental image corresponding to the computational domain (half of an image of Fig. 1) is also shown. (b) Forces and moments acting on an arc starting from the origin.

The initially straight paper extends as the liquid begins to permeate into the paper from the tube and eventually buckles into the second mode that is stabilized by the capillary. As observed, the wetted domain, $0 < X < L_w(t)$, has uniform thickness τ_s and Young's modulus E_s while the dry domain, $L_w < X < L$, has thickness τ_d and Young's modulus E_d. For each domain, we set up the geometrically nonlinear post-buckling equations of force and moment equilibrium and geometric compatibility.[17]

The center line of the paper strip expands on being wet and has a stretch defined by $r_i = \mathrm{d}S_i/\mathrm{d}X$, where S is the length of the strip measured from the origin and $i = 1,2$ correspond to the wet and dry regions, respectively. Denoting the horizontal and vertical deformations of the strip at X by $U(X)$ and $W(X)$, respectively, we have $\mathrm{d}U_i/\mathrm{d}X = r_i\cos\theta_i - 1$ and $\mathrm{d}W_i/\mathrm{d}X = r_i\sin\theta_i$. Then, force equilibrium perpendicular to the sheet, as shown in Fig. 7(b), leads to

$$\hat{N}_i + \hat{P}\cos\theta_i + \hat{V}\sin\theta_i = 0, \tag{4}$$

where $\hat{N}_i$ is the internal tension given by $\hat{N}_i = E_iA_i(r_i - 1 - \epsilon_{h,i})$, and $\hat{P}$ and $\hat{V}$ are the horizontal and the vertical reaction at the ends, respectively. The hygroexpansive strain, ϵ_h, in the wet domain is assumed to be ϵ_c at saturation thus $\epsilon_{h,1} \approx 0.0156$ and $\epsilon_{h,2} = 0$. Similarly, moment equilibrium yields

$$\hat{M}_i + \hat{P}W_i - \hat{V}(U_i + X) = 0, \tag{5}$$

where $\hat{M}_i = E_iI_i\mathrm{d}\theta_i/\mathrm{d}X$ is the moment at $(X + U_i, W_i)$, and the area moment of inertia, I_i, in each domain is given by $I_1 = b\tau_s^3/12$ and $I_2 = b\tau_d^3/12$.

Nondimensionalizing the lengths, forces, and moments as $(x, s_i, u_i, w_i) = \frac{1}{L}(X, S_i, U_i, W_i)$, $(P, V) = \frac{L^2}{E_2I_2}(\hat{P}, \hat{V})$, and $M_i = \frac{L}{E_2I_2}\hat{M}_i$ yields the following dimensionless governing equations for the shape of a post-buckled wet paper:

$$\begin{aligned}
\frac{\mathrm{d}s_i}{\mathrm{d}x} &= r_i, \\
\frac{\mathrm{d}u_i}{\mathrm{d}x} &= r_i\cos\theta_i - 1, \\
\frac{\mathrm{d}w_i}{\mathrm{d}x} &= r_i\sin\theta_i, \\
\frac{\mathrm{d}\theta_1}{\mathrm{d}x} &= \frac{1}{\beta}\left[-Pw_1 + V(x + u_1)\right], \\
\frac{\mathrm{d}\theta_2}{\mathrm{d}x} &= -Pw_2 + V(x + u_2),
\end{aligned} \tag{6}$$

where $r_1 = -(P\cos\theta_1 + V\sin\theta_1)/(\beta\lambda_1^2) + \epsilon_{h,1} + 1$, $r_2 = -(P\cos\theta_2 + V\sin\theta_2)/\lambda_2^2 + \epsilon_{h,2} + 1$, $\beta = (E_1I_1)/(E_2I_2)$, and $\lambda_i = L(A_i/I_i)^{1/2}$ with A_i being the cross-sectional area: $A_1 = b\tau_s$ and $A_2 = b\tau_d$.

To complete the formulation of the problem, we need to specify some boundary and matching conditions that accompany Eq. (6) to determine the eight constants of integration and the unknown reactions P and V. The paper strip is pinned at $x = 0$ so that the corresponding boundary conditions are $s_1(0) = 0, u_1(0) = 0$, and $w_1(0) = 0$. At the other end, $x = 1$, the sheet is clamped thus we may write $u_2(1) = 0$, $w_2(1) = 0$, and $\theta_2(1) = 0$. These six boundary conditions must be supplemented by matching conditions at the interface $x = l_w = L_w/L$ given by the continuity of the stretching, deflection, and slope, i.e., $s_1(l_w) = s_2(l_w)$, $u_1(l_w) = u_2(l_w)$, $w_1(l_w) = w_2(l_w)$, and $\theta_1(l_w) = \theta_2(l_w)$. Although l_w designates the arc length of the wetted portion, we approximate the original position of the wet front on the x-axis to be equal to l_w for mathematical simplicity, with an error of 1.56%, the maximum hygroexpansive strain. We then employ a shooting method[18] to numerically solve the system with MATLAB.

To validate our numerical solutions, we first compare the shapes of an entirely wet paper predicted by our simulation and analytical modeling. For relatively small strains, $\epsilon_c = 0.0156$, a linear analysis leads to the shape of a buckled homogeneous beam pinned at one end and clamped at the other as[19]

$$w = \frac{V_0}{P_0}\left[1.024\sin(4.493x) + x\right]. \tag{7}$$

Since the vertical and horizontal loads at either end, V_0 and P_0, respectively, cannot be determined in the linear theory, we substitute the values obtained by our numerical computation in Eq. (7) to plot the analytical solution. Figure 8 shows that the numerically predicted beam shape matches the analytical solution for a homogeneous beam.

Now we compute the shape evolution of the paper strip as imbibing water from a capillary tube. Since the propagation speed of the wet front is known *a priori*, the beam shape at each instant is given by the solution of Eq. (6) with a given l_w. Figure 9 compares the beam shapes that are experimentally observed and theoretically computed for various l_w showing that the agreement between theory and experiment in the early stages is excellent while differing slightly in later stages due to time-dependent viscoelastic properties of paper and gravity. For a suspended beam with pinned-fixed ends, the maximum deflection under uniform gravitational loading is given by $\delta_g = fL^4/(184.6EI)$,[20] where f is the linear force density, $f = \rho g b\tau_s n/\phi_s$ with ρ and g being the density of saturated paper and the gravitational acceleration, respectively. For $L = 20$ mm, $\delta_g = 64$ μm. Although much smaller than the maximum deflection due to hygroexpansive buckling,[19] $\delta_h \approx (1.956/\pi)\epsilon_h^{1/2}L = 1.56$ mm, it plays a limited role in vertical deflection in late stages. We also note that imperfect elastic behavior of paper due to its viscoelastic properties dependent on wetting time and water content was reported earlier.[8]

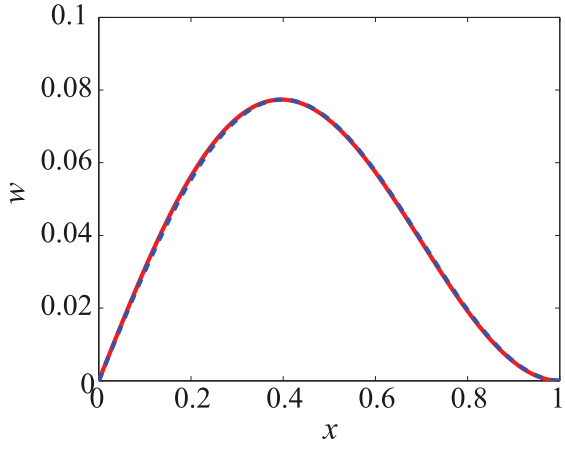

FIG. 8. Comparison of the shapes of entirely saturated homogeneous beams predicted by the numerical computation (red solid line) and the linear buckling theory complemented by the numerically computed coefficients (blue dashed line).

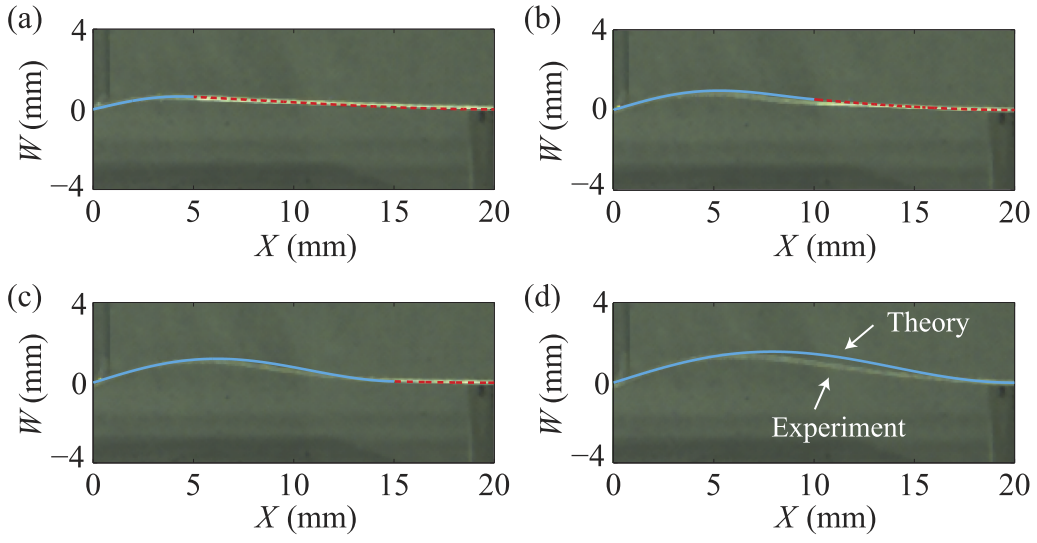

FIG. 9. Shape evolution of the paper strip imbibing water from a capillary tube. Blue lines and red dots correspond to the theoretically computed shapes of the wet and dry portions, respectively. (a) $L_w = 5$ mm, $t = 3.1$ s. (b) $L_w = 10$ mm, $t = 14.3$ s. (c) $L_w = 15$ mm, $t = 37.7$ s. (d) $L_w = 20$ mm, $t = 66.0$ s.

Figure 10 shows the theoretical temporal evolution of the beam shape and reaction forces. The strain in the wetted portion, defined as $\epsilon_1 = [s_1(l_w) - l_w]/l_w$, in Fig. 10(a), starts at 1.18% when the buckling initiates, increases sharply until $l_w = 0.14$, and then gradually saturates to 1.54%. Considering that the hygroexpansive strain in the unconstrained condition, $\epsilon_h = 1.56\%$, the suspended paper strip tends to stretch almost as if it were not compressed when completely wet. The extensional strain of the dry portion, defined as $\epsilon_2 = [s_2(1) - s_2(l_w) - l_d]/l_d$, where $l_d = 1 - l_w$, is nearly zero. The y-directional displacement w in Fig. 10(b) is similar to that of a buckled uniform beam in the early and late stages, but in the intermediate stages, the dry portion is less curved than the wet portion because of the large difference in the bending stiffness EI. We have found that the maximum deflection occurs in the dry portion from the beginning until $l_w = 0.14$, while it is located in the wet portion afterwards.

In Figure 10(c), we show the slope of the beam and observe that the wet portion rotates far more than the dry portion due to the softening of wet paper. The reaction forces at either end are plotted in Fig. 10(d). The horizontal force decreases sharply in the early stages as the beam deflects from the initially straight configuration and the soft wet portion grows. The final horizontal load $P = 1.17$ differs from the critical buckling load of a homogeneous wet paper constrained by pinned-fixed ends, 1.18, only by 1%, which is consistent with the fact that the final strain of the constrained paper strip is close to the inherent hygroexpansive strain. The vertical reaction reaches a local minimum at around $l_w = 0.14$, which is consistent with the instant when the location of maximum deflection moves from the dry to wet portion. The maximum of V occurs at $l_w = 0.42$, where the inflection point of the beam shape is found to move from the dry to wet portion.

The nondimensional shape of the paper strip, $w(x)$, depends on the dimensionless parameters ϵ_h, β, λ_1, and λ_2 as well as l_w. Upon finding that the effects of variation of λ_1 and λ_2 are negligible, we vary the values of ϵ_h and β while l_w is fixed to a representative value 0.5, to investigate their influence on the shape of a partially wet strip. Figure 11(a) shows that the paper deflection increases with the hygroexpansive strain ϵ_h, which is intuitively obvious. In Fig. 10(b), we see that as the ratio of the bending stiffness of the wet portion to the dry portion, β, increases, the maximum deflection of the paper strip increases and approaches that for a homogeneous dry beam that buckles with a uniform strain ϵ_h.

Finally, we note that the magnitude of post-buckling deflection δ and curvature κ can be simply related to the expansive strain, ϵ_h, and its initial length, L, using a scaling analysis. The increase of the beam length for the wetted length $L_w = l_w L$ can be scaled as $\Gamma \sim \epsilon l_w L$. It is accommodated

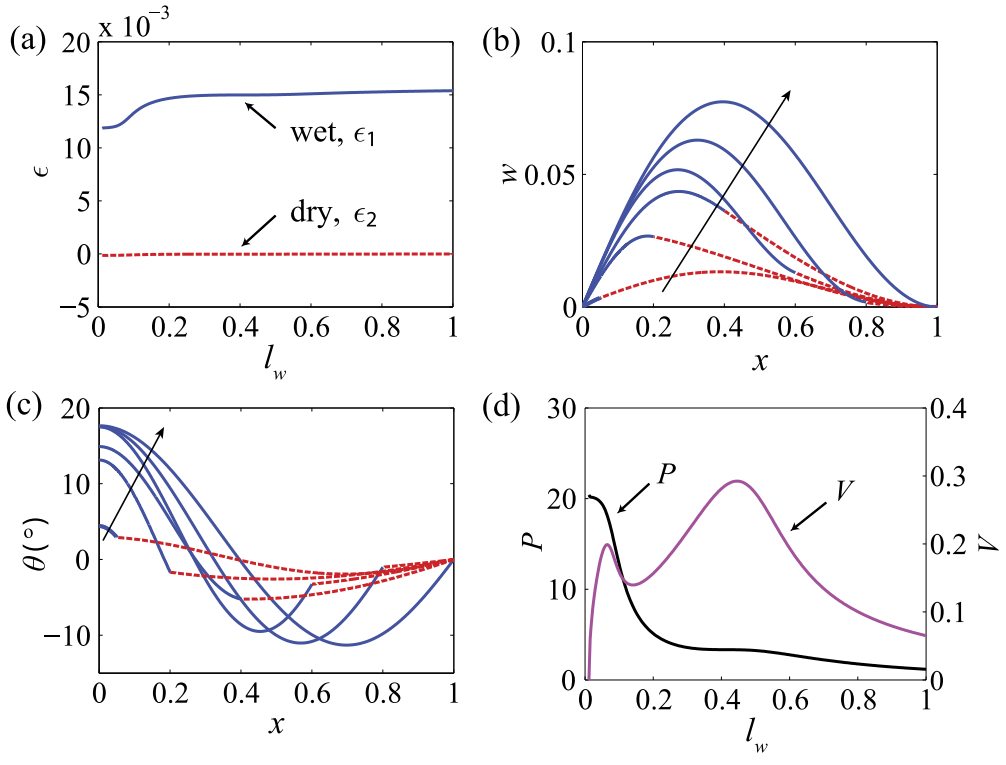

FIG. 10. Theoretical temporal evolution of the beam shape and reaction forces, caused by increase of l_w. (a) The evolution of strains of the wet and dry portions with increase of l_w. (b) Displacement in y-direction. Blue solid lines and red dashed lines correspond to the wet and dry portions, respectively. l_w increases in the direction of the arrow taking the values 0.05, 0.2, 0.4, 0.6, 0.8, and 1. (c) Deflection angle with respect to the x-axis. Symbols are the same as those in (b). (d) The reaction forces in the horizontal (P) and vertical (V) directions versus l_w. Note that the computational results start from $l_w = 0.012$ to show the post-buckling responses.

by the deflection resulting from buckling, so that we may write $\Gamma \sim \int_0^L [(1+y'^2)^{1/2} - 1]\mathrm{d}x \sim y'^2 L$. Since $y' \sim \delta/L$, we get $\delta \sim (\epsilon l_w)^{1/2} L$ and $\kappa \sim y'/L_w \sim (\epsilon l_w)^{1/2}/L_w = (\epsilon/l_w)^{1/2}/L$. To test whether these scalings hold for partially wet paper, we plot the maximum deflection, δ_m, and the maximum curvature, κ_m, of a filter paper that is wet up to $l_w = [0.2 - 1]$ versus $(\epsilon_h l_w)^{1/2} L$ and $(\epsilon_h/l_w)^{1/2}/L$,

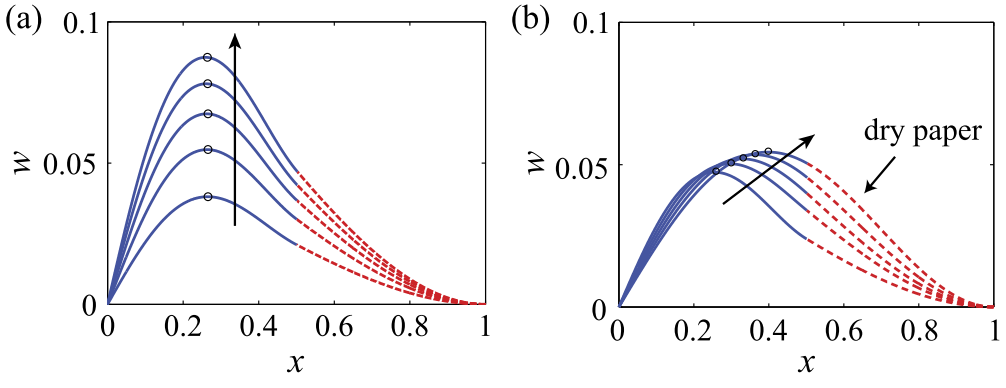

FIG. 11. Effects of dimensionless parameters on the shape of a partially wet paper with $l_w = 0.5$, $\lambda_1 = 384$, and $\lambda_2 = 304$, corresponding to the filter paper with $L = 20$ mm. Maximum deflection is marked as a circle in each curve. (a) ϵ_h increases in the direction of the arrow taking the values 0.01, 0.02, 0.03, 0.04, and 0.05, while β is fixed to 1/17. (b) β increases in the direction of the arrow taking the values 1/20, 1/10, 1/5, 1/2, and 1, while ϵ_h is fixed to 0.0156. In all the cases, we assume that the deflection is within the elastic limit.

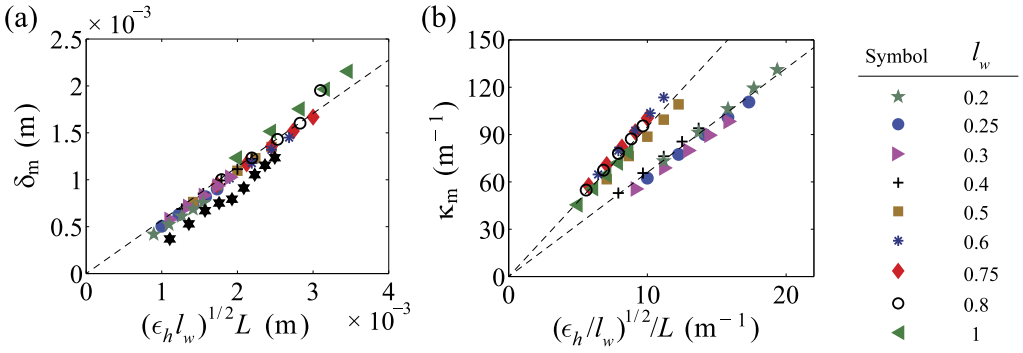

FIG. 12. Scaling relations of the shape of a partially wet paper. (a) Maximum deflection versus $(\epsilon_h l_w)^{1/2} L$. The slope of the best fitting line is 0.57. (b) Maximum curvature versus $(\epsilon_h / l_w)^{1/2} / L$. The slopes of the best fitting lines for the data of $l_w \le 0.4$ and $l_w \ge 0.5$ are 6.5 and 9.6, respectively. For each symbol corresponding to different l_w, ϵ_h varies from 0.01 to 0.03. The black stars in (a) correspond to the experimental results of the present study.

respectively, in Fig. 12. All the deflection data are collapsed onto a single master curve as shown in Fig. 12(a). Furthermore, the maximum curvature collapses onto two distinct straight lines depending on l_w, Fig. 12(b). We see that the curvature of a partially wet beam abruptly increases as l_w grows from approximately 0.4 to 0.5, which also corresponds to the value where the inflection point of the beam shape moves from the dry to wet portion as mentioned previously.

IV. CONCLUSIONS

To understand the geometry and mechanics of the buckling and bending of wet paper, we have characterized the hygroexpansive nature of filter paper and analyzed the shape evolution of a paper strip. The fast thickness-wise swelling compared to the in-plane imbibition allowed us to model the dynamics of deformation using a quasi-static approximation.

Although we have considered the swelling and buckling of a paper strip due to one-dimensional Washburn-like in-plane imbibition that occurs for most of time range, the thickness-wise swelling and in-plane imbibition were observed to be strongly coupled in the very early stages. Understanding this process requires the simultaneous consideration of poroelastic deformation of hygroexpansive cellulose network and water imbibition through pores of time-varying volume, which is currently under investigation.

ACKNOWLEDGMENTS

This work was supported by the National Research Foundation of Korea (Grant Nos. 2015001863, 2014048162, and 2015035006, H.Y.K.), the MacArthur Foundation (L.M.), and the Wyss Institute for Biologically Inspired Engineering (H.Y.K. and L.M.). The administrative support of SNU IAMD is acknowledged.

[1] N. Bowden, S. Brittain, A. G. Evans, J. W. Hutchinson, and G. M. Whitesides, "Spontaneous formation of ordered structures in thin films of metals supported on an elastomeric polymer," Nature **393**, 146-149 (1998).
[2] M.-W. Moon, S. H. Lee, J.-Y. Sun, K. H. Oh, A. Vaziri, and J. W. Hutchinson, "Wrinkled hard skin on polymer substrates induced by focused ion beam irradiation," Proc. Natl. Acad. Sci. U. S. A. **104**, 1130-1133 (2007).
[3] K. Efimenko, M. Rackaitis, E. Manias, A. Vaziri, L. Mahadevan, and J. Genzer, "Nested self-similar wrinkling patterns in skins," Nat. Mater. **4**, 293-297 (2005).
[4] J. Huang, M. Juszkiewicz, W. H. de Jeu, E. Cerda, T. Emrick, N. Menon, and T. P. Russell, "Capillary wrinkling of floating thin polymer films," Science **317**, 650-653 (2007).
[5] D. P. Holmes, M. Roché, T. Sinha, and H. A. Stone, "Bending and twisting of soft materials by non-homogenous swelling," Soft Matter **7**, 5188-5193 (2011).
[6] J. I. Siddique, D. M. Anderson, and A. Bondarev, "Capillary rise of a liquid into a deformable porous material," Phys. Fluids **21**, 013106 (2009).
[7] E. Reyssat and L. Mahadevan, "How wet paper curls," Europhys. Lett. **93**, 54001 (2011).

[8] S. Douezan, M. Wyart, F. Brochard-Wyart, and D. Cuvelier, "Curling instability induced by swelling," Soft Matter **7**, 1506-1511 (2011).
[9] J. Y. Chung, H. King, and L. Mahadevan, "Evaporative microclimate driven hygrometers and hygromotors," Europhys. Lett. **107**, 64002 (2014).
[10] D. Topgaad and O. Söderman, "Diffusion of water absorbed in cellulose fibers studied with 1H-NMR," Langmuir **17**, 2694-2702 (2001).
[11] J. A. Enderby, "Water absorption by polymers," Trans. Faraday Soc. **51**, 106-116 (1955).
[12] A. Schröder and D. Bensarsa, "The Young's modulus of wet paper," J. Pulp Pap. Sci. **28**, 410-415 (2002).
[13] S. Timoshenko, "Analysis of bi-metal thermostats," J. Opt. Soc. Am. **11**, 233-255 (1925).
[14] M. Alava and K. Niskanen, "The physics of paper," Rep. Prog. Phys. **69**, 669-723 (2006).
[15] E. W. Washburn, "The dynamics of capillary flow," Phys. Rev. **17**, 273-283 (1921).
[16] A. Pandey, D. E. Moulton, D. Vella, and D. P. Holmes, "Dynamics of snapping beams and jumping poppers," Europhys. Lett. **105**, 24001 (2014).
[17] S. Li, Y.-H. Zhou, and X. Zheng, "Thermal post-buckling of a heated elastic rod with pinned-fixed ends," J. Therm. Stresses **25**, 45-56 (2002).
[18] H. P. Williams, P. F. Brain, and A. T. Sain, *Numerical Recipes - The Art of Scientific Computing* (Cambridge University Press, London, 1986).
[19] R. M. Jones, *Buckling of Bars, Plates, and Shells* (Bull Ridge Publishing, Blacksburg, 2006).
[20] F. A. Leckie and D. J. Dal Bello, *Strength and Stiffness of Engineering Systems* (Springer, New York, 2009).